Nanoscale

PAPER

View Article Online
View Journal | View Issue

Cite this: *Nanoscale*, 2026, **18**, 1643

Local networks of electrical conductance in hybrid gold nanoparticle–polymer films

Sukanya Das, [a] Michael A. H. Klos, [a,b] Tobias Kraus [a,b] and Roland Bennewitz *[a,c]

Received 14th October 2025,
Accepted 5th December 2025

DOI: 10.1039/d5nr04335b

rsc.li/nanoscale

Inks of gold nanoparticles with stabilizing and conducting polymer shells are promising materials for printed electronics. Local measurements of their electrical properties at the single-particle scale are required to understand the relationship between the particle network and electrical functionality. Herein, we report on conductive atomic force microscopy (cAFM) on films produced from hybrid Au nanoparticles that carry a covalently bound shell of the conducting polymer poly(3,4-ethylenedioxythiophene) polystyrene sulfonate (PEDOT:PSS) and are distributed in a non-conductive matrix of polyvinyl alcohol (PVA). Current maps reveal the clustering of particles into electrically well-connected local networks and allow us to quantify the contact resistance between particles or clusters of particles. We find that the contact resistance between particles inside clusters is lower than those between clusters, indicating a hierarchical layer structure. By comparing inkjet-printed thicker bulk films and drop-cast films of single- or few-layer thickness, the experimental results offer valuable insights into the relationship between the structure of nanoparticle networks and the electrical conductance in these hybrid systems.

Introduction

Hybrid nanoparticles that combine inorganic nanocores with organic shells have found widespread applications in flexible electronics. Their size-dependent, tunable properties have been exploited in light emitting diodes,[1] memory devices,[2] solar cells,[3] sensors,[4] anti-reflective surfaces[5] and various other low cost, large-area printable electronics.[6,7]

Hybrid nanoparticles with metal cores and non-conductive ligands are the basis of most established inkjet-printable inks for electrically conductive traces.[8] Silver or gold cores are coated with ligand shells of amines, thiols or phosphines with small molecular weights, citrate ions, or polymers such as polyvinylpyrrolidone to ensure their dispersibility in a solvent.[9] These ligands are electrically insulating and cause tunnel barriers. Thus, the conductivity of the printed films is low after drying and temperatures in the range of 150–400 °C, laser exposure,[10] or microwave treatment[11] is necessary to obtain metallic films. The organic layers desorb and enable the coalescence of neighboring metal cores, yielding conductivities close to those of vacuum-deposited thin films.[9]

Nanoparticle coalescence increases conductivity, but the required temperatures limit the choice of flexible substrates. Polymer substrates deform or degrade at temperatures above their glass transition temperatures. In addition, the loss of the particles' individual nature removes the possibility of tuning properties through interfacial engineering. It is attractive to retain the particulate nature of films for applications that exploit interfacial or small-scale electronic effects. This has prompted a search for conductive ligand shells that enable electronic conduction without tunneling through insulating ligand shells.

Conjugated polymers can replace insulating ligands and form conductive interfaces between conductive cores. The first step towards such hybrids was taken using semiconductor nanoparticles, where Zorn *et al.* coated CdSe@ZnS quantum dots with a block copolymer (BCP) comprising a triphenylamine-based semiconductor and a short reactive ester block.[12] This concept was then transferred to metals such as gold and silver, resulting in conducting hybrid and composite materials.[13–17] The choice of polymer–core combination and the tuning of the metal core–polymer shell interface enable the engineering of opto-electronic properties. Optimized surface chemistries improved the effective binding of polymer chains in the hybrid core–shell structures and enhanced the connectivity between the interfaces of metal cores.[18,19] Understanding the structural and electrical properties of the hybrid interface is crucial for the further enhancement of electrical transport in particle-based material systems.

[a]*INM – Leibniz-Institute for New Materials, 66123 Saarbrücken, Germany.*
E-mail: roland.bennewitz@leibniz-inm.de
[b]*Colloid and Interface Chemistry, Saarland University, 66123 Saarbrücken, Germany*
[c]*Department of Physics, Saarland University, 66123 Saarbrücken, Germany*

Conjugated polymers that effectively bind to the surface of gold cores enhance the electronic conduction across the metal–polymer interface.[20] Reiser and coworkers have demonstrated conductive inks of gold-nanorods with polythiophene coatings that can be produced by sintering-free techniques, retaining chemical stability and good electron conductivity.[21] Gold nanoparticles with PEDOT:PSS shells yielded printable inks with an average low resistivity of $\approx 4.42 \times 10^{-5} \pm 7.57 \times 10^{-6}$ Ωm (ref. 15) and potential for large-scale solution processing. The mechanical flexibility of thin films made from these highly conductive nanoparticle inks was improved by the addition of low contents of poly(vinyl alcohol) (PVA).[22] The PEDOT:PSS polymer stabilizes the AuNPs and provides conductivity after processing without a sintering step, whereas PVA adds improved mechanical stability to the nanocomposite film. These hybrid inks of AuNPs are promising candidates for flexible conducting electronic circuits.

It has been shown for different hybrid materials composed of nanocrystals that the range of hopping transport and metal–insulator behavior can be tuned by varying the contact area of metal/semiconducting nanocores and by changing the filler contents or the doping concentration.[23–26] Several experimental techniques, *e.g.*, scanning tunneling microscopy or electron microscopy, have been used for electrical measurements at the nanoscale.[27–29] There are previous reports of nanoscale electrical characterization of assemblies of conductive metal nanoparticles that can be used in electronic circuits.[30–32] However, understanding the electrical conductivity of an ensemble of NPs in hybrid films on the macroscale requires data on the connectivity of particles with a diverse distribution of size or energy barriers. Thus, the study of electrical transport between two single nanoparticles at the molecular level (~nm) may not predict the macroscopic conductivity on the scale of experimental devices (~few mm). The collective behavior of hybrid particle networks at intermediate length scales provides relevant information on mesoscale transport properties for designing optimized electronic devices.

In this work, conductive atomic force microscopy (cAFM) has been performed on thin films of hybrid nanoparticle ink to study electrical current features on the mesoscale. The manifestation of collective effects of particle clusters is discussed in terms of resistance maps. Despite the experimental limitations of contact-mode AFM on soft materials under ambient conditions, the right combination of cantilever stiffness, tip material, and scanning parameters allows the quantification of electrical transport features on the hybrid ink film surface. We present a comparative study of local current features of hybrid bulk films, which are prepared by inkjet printing on foil to represent applications in flexible electronics, and of hybrid thin films on glass, which exhibit monolayer islands and allow for detailed imaging in conductive AFM. Clustering of particles in the film leads to subnetworks in the resistance depending on the ink concentration and film thickness. The findings help to understand the connectivity of hybrid nanoparticles and the mesoscale electrical transport in hybrid thin films.

Materials and methods

For this study, two types of films were prepared from an ink prepared from AuNPs with an average radius of 80 nm and a polydispersity of 15% as estimated from dynamic light scattering. Particles were stabilized with a covalently bound PEDOT:PSS shell[22] and redispersed in an aqueous solution of PVA (molecular weight of 89 000–98 000, 99+% hydrolyzed, Sigma-Aldrich, Germany). Briefly, gold nanoparticles were synthesized using a seeded growth route and a sacrificial ligand that was replaced with PEDOT:PSS. The concentrated ink was diluted to 130 mg mL^{-1} gold. Thermogravimetric analysis indicated a gold content of 97.4%, corresponding to approximately 2.6% PEDOT:PSS or approximately 3.5 mg mL^{-1}. Details of the particle synthesis and ink formulation are given in a previous publication.[22] The diluted hybrid particle dispersion was mixed with a 5 wt% PVA stock solution to achieve a PVA-to-Au volume ratio of 10 vol% PVA and 90% vol% Au in all inks and all films.

A bulk film was produced by inkjet printing on a flexible, transparent polyethylene terephthalate (PET) substrate. The ink and the printing procedure, which are devised for application in the production of flexible electronics, are described in ref. 22. To produce a few-layer film, the same hybrid ink was diluted with MilliQ water to a solid content of 10 mg ml^{-1} and then pipetted onto a plasma-cleaned glass substrate between two fixed boundaries separated by 2 mm. All samples were dried at room temperature for one week. The inkjet-printed bulk films had a thickness of approximately 1 μm, while the drop-cast few-layer films on glass varied in thickness across the sample. Here, we study the areas of the films that exhibit a thickness of single particles or, locally, of a few particles.

Conductive AFM was performed with a JPK Nanowizard 3 (Bruker, Germany) using electrically conducting Pt/Ir-coated Si tips (SCM PIT V2 from Bruker). As discussed in the Results and discussion section, the cAFM measurements were performed after adding a series resistor (~1 MΩ) to the concentrated hybrid ink film externally with Ag conductive paste. All experiments were performed in air at room temperature. Constant bias voltages of 50 mV–1.2 V were applied to the conducting tip with respect to the ground for the scans. High-resolution topography images were recorded in tapping mode with PPP-NCL tips (Nanosensors). The data were processed using JPK data processing software, Origin 9.1 and Gwyddion 2.63.

Results and discussion

The topographies of typical surfaces of the bulk and few-layer films produced with high- and low-concentration inks of AuNPs@PEDOT:PSS/PVA are depicted in Fig. 1a and b.

The surface of the inkjet-printed bulk film exhibits a dense packing of interconnected particles, as shown in Fig. 1a, and has an approximate root-mean square (rms) roughness of 22 nm. The few-layer film is less dense and has a thickness of only one or two layers of nanoparticles on the glass substrate,

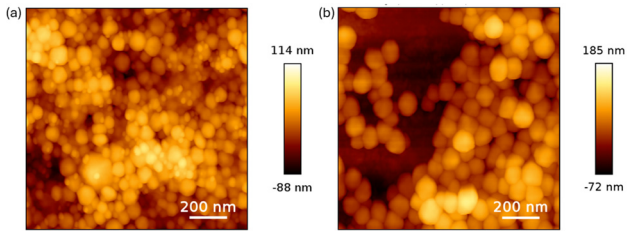

Fig. 1 Surface topography of hybrid gold nanoparticle films recorded in tapping mode AFM. (a) Inkjet-printed bulk film with a thickness of 1 μm. (b) Single and double layers of particles in an area of a few-layer film.

which is imaged between particles, as shown in Fig. 1b. The rms roughness in this area of the few-layer film is 39 nm. Additional topography and phase maps recorded on the bulk films and the few-layer films are provided in Fig. S1 of the SI.

The local current images recorded using cAFM reveal the nanoscale distribution of electrical conductance of the materials. Fig. 2a and b show the experimental setup of cAFM for the bulk film surfaces. A typical current map over an area of 1 μm × 0.5 μm is shown in Fig. 2c. Individual nanoparticles are resolved in this current map. Most particles show a common maximum value of current, but some single particles or groups of a few neighboring nanoparticles show a lower but locally constant current. The map indicates that the measured current is determined predominantly by the electrical connection of each nanoparticle to the rest of the film, rather than by fluctuations of the tip–particle contact across that nanoparticle. The typical line profile in Fig. 2d identifies the maximum current magnitude with 120 nA as the saturation limit of the given current amplifier. To protect the amplifier

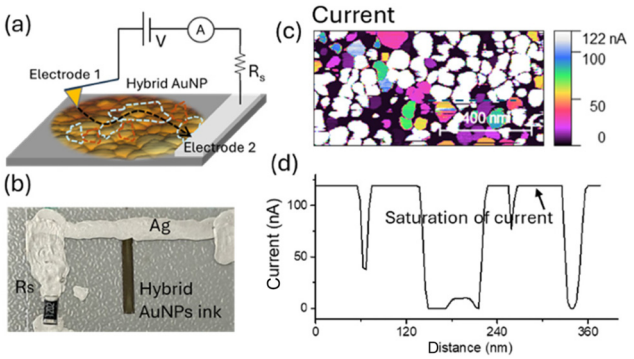

Fig. 2 Experimental setup and typical result of cAFM. (a) Schematic of the cAFM with the Pt/Ir coated conductive nanotip as one electrode and silver paste as the second electrode. The current (black dashed line) flows from electrode 1 to electrode 2 through the particle networks of different sizes and conductance. (b) Photograph of the inkjet-printed bulk film of AuNPs@PEDOT:PSS/PVA deposited on a flexible PET sheet and its connection by Ag paste with a series resistor R_s. (c) Current map of a small area recorded without a series resistor in the circuit (bias voltage: 20 mV). The regions with lower current are associated with the purple/green areas, while the highest currents are observed in the blue/white regions. (d) Current profile over the marked line in (c) with current magnitudes reaching the saturation limit of the amplifier.

and to analyze any current variations across the surface and between these nanoparticles showing a maximum current, a resistor $R_s \sim 1$ MΩ is connected in series with the ink sample. The inkjet-printed bulk film deposited on flexible PET with an additional resistor R_s in series is shown in Fig. 2b. Upon addition of the series resistor, the current profile over the surface curvature of each nanoparticle is observed to be still nearly constant (Fig. S2 in the SI). This finding confirms that the measured current is dominated by the resistance between particles and the network rather than the negligible contact resistance between the tip and particle.

Overview topography and current maps recorded simultaneously in contact mode AFM at the 25 μm length scale are shown in Fig. 3a and b for a bulk film. The surface has a rms roughness of ~30 nm. The current map exhibits a local variation at the small scale and a few sub-micrometer-sized areas with no current. The maximum current of ~40.7 nA is limited by the series resistor. Detailed topography and current maps with the resolution of individual particles are shown in Fig. 3c and d. The images are distorted by abrupt lines in the horizontal direction of fast scanning. These lines are artefacts that appear when bits of film material are suddenly transferred to the tip. Despite this inherent challenge of contact-mode AFM on soft materials, the structure of the films can be imaged reproducibly. Additional contact-mode current maps recorded on various areas of bulk films are provided in Fig. S3 of the SI. The current map shows that most particles have a current value close to the maximum value, indicating that they are electrically well connected to the overall network of the film. Some particles and depressions in between particles show no current and, thus, appear to be disconnected from the underlying network. A few single particles and small assemblies of particles exhibit different but constant current magnitudes. The current values across these single particles and assemblies are reflected as peaks in the corresponding current histogram in Fig. 3d. Similar current maps of particles in a closed film have been reported before for semiconducting ZnO particles.[25]

To quantify the contact resistance between particles showing different current magnitudes, we calculated the difference in path resistance to any two points 1 and 2 where the cAFM tip contacts the surface. V_{appl} is the voltage applied to the cAFM setup including the sample and the series resistor. Then the difference in resistance between the two points 1 and 2 is given by:

$$\Delta R = V_{appl} \frac{I_2 - I_1}{I_2 I_1} \quad (1)$$

where ΔR is the difference in total resistance from the contact electrode to each of the two points. An equivalent circuit with derivation of eqn (1) is provided in Fig. S4 of the SI. Resistance maps are shown in Fig. 3e and f. To calculate values for these maps, we used $V_{applied}$ = 50 mV, a value of I_2 = 40.7 nA, which is the maximum current in this map, for an external reference point (see the scheme in Fig. 3f) where current enters this area of the sample, and I_1 from each point of the current map (Fig. 3d). In Fig. 3e, the electrically well-connected particles

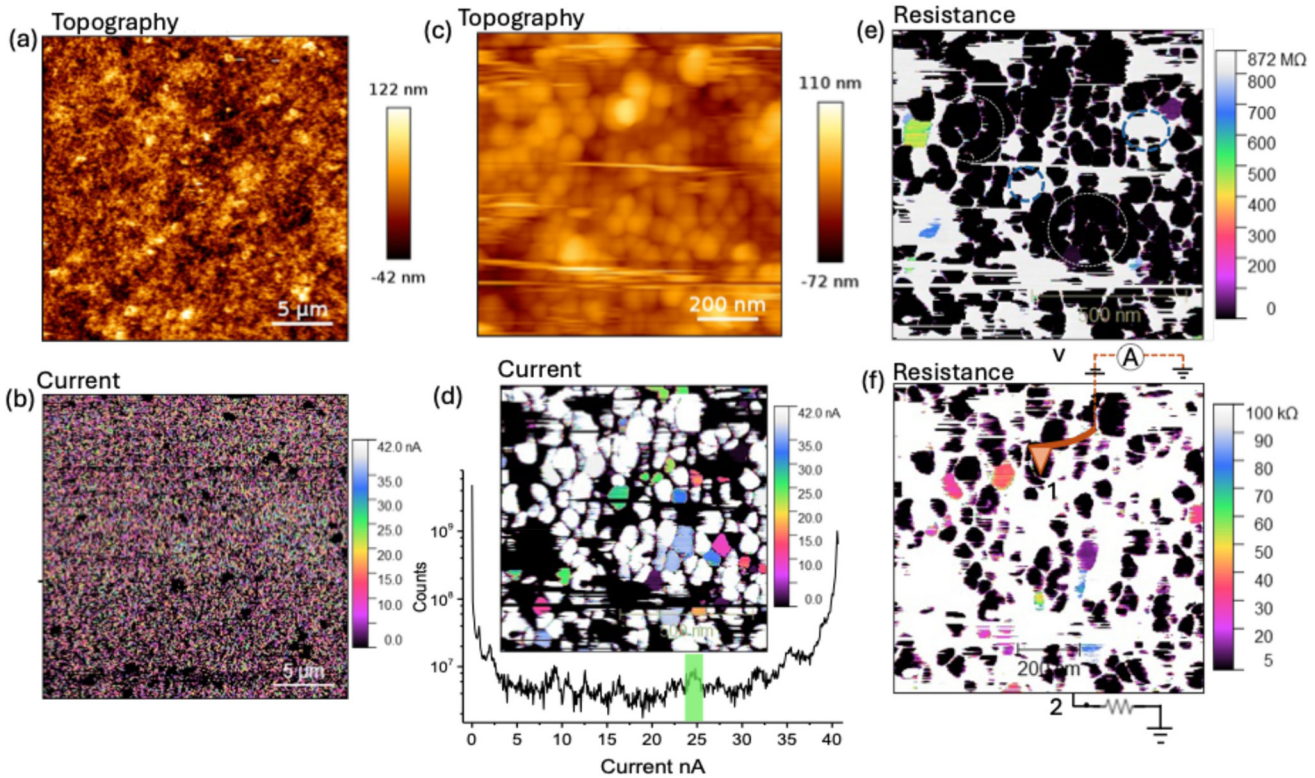

Fig. 3 Conductive AFM on the surface of a bulk film (bias voltage: 50 mV). (a and b) Topography and current maps for an area of 25 µm × 25 µm. (c and d) Detailed topography and current maps for a scan area of 1 µm × 1 µm. A corresponding current histogram is included in (d). The area marked in green represents the distinct green regions in the current map. Topography and current maps were recorded simultaneously. (e and f) Maps of resistance for the measurement presented in (d). The resistance to tip position 1 was calculated with respect to an external point 2 (see the text). (e) Color scale up to 872 MΩ. The white-dotted circles indicate well-connected nanoparticles, while the blue-dotted circles indicate high resistance regions. (f) Color scale up to 100 kΩ.

appear as black regions with negligible resistance with respect to the external reference points. A small number of particles are only weakly connected to the conducting network and exhibit large resistances of hundreds of MΩ, compared to their electrically well-connected neighbors.

Since these particles are surrounded by well-connected particles with vanishing resistance, we assume that the difference in resistance indicates the contact resistance between a neighboring well-connected particle and the particle with higher resistance. To visualize lower contact resistances between electrically well-connected particles, the same data are shown again in Fig. 3f with the resistance scale from 5 kΩ to 100 kΩ. We observe that a fraction of single nanoparticles on the surface of the conductive network shows a resistance difference of some tens of kΩ with respect to their neighbors. We conclude that the contact resistance between the conductive network of particles and single less-well-connected particles on its surface can take any value between a few kΩ and hundreds of MΩ. We want to stress that the overall resistance of stripes of bulk films like those in Fig. 2b is a few hundreds of Ω.[22] We conclude that the three-dimensional network in the bulk film offers conductive pathways with much lower inter-particle contact resistances than those observed for weakly connected particles on the surfaces. While there is no experimental means to probe local resistance in the bulk, cAFM has the capability to probe resistance across a two-dimensional network of particles. We therefore prepared films with low-concentration ink, which consist mostly of a single or double layer of particles.

The topography and current map for an overview of a few-layer film are shown in Fig. 4a and b. The topography reveals a flat arrangement of particles with some elevated islands, which probably consist of small patches of an additional layer of particles. These elevated islands caused instabilities in the scanning process, making a quantitative roughness analysis at this scale difficult. The current magnitudes are 20 times lower compared to bulk films, as shown in Fig. 3, despite a 20 times higher bias voltage. This current was recorded without a series resistor and indicates that the overall resistance of these films is much higher than that of bulk films. The current map exhibits distinct regions of equal current with a lateral extension of several micrometers, including areas with no current at all. We tentatively conclude that these distinct regions are formed by two-dimensional clusters of electrically well-connected particles, which, however, are interconnected by links of higher contact resistance. The constant current level within each distinct region is highlighted by peaks in the enclosed current histogram.

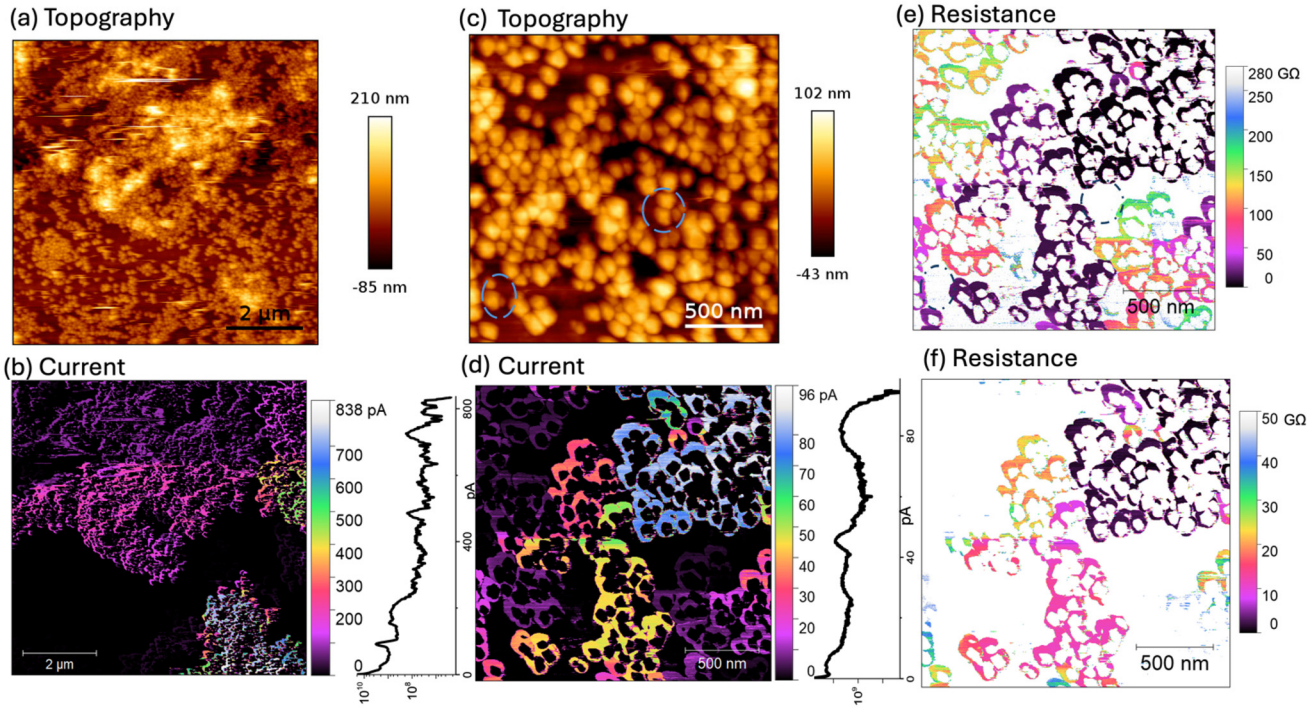

Fig. 4 Conductive AFM on a few-layer film (bias voltage: 1.2 V). (a and b) Topography and current maps of a large area (8 µm × 8 µm). (c and d) Topography and current maps of a small area (2 µm × 2 µm). Topography and current maps were recorded simultaneously. (e and f) The resistance map corresponding to (d) with color scales up to 280 GΩ and 50 GΩ, respectively. The blue-dotted circles in (c) and (e) indicate nanoparticles that are electrically disconnected from the conductive network.

This structure is confirmed by the detailed maps in Fig. 4c and d. The stable contact-mode imaging reveals an rms roughness of 26.3 nm and a single- or double-layer arrangement of particles with interspersed areas of the substrate without any particles. Distinct clusters of particles exhibit a constant current level with a sudden change in current between adjacent particles belonging to different clusters. While we cannot prove that the resistive connection between clusters is mediated by a single particle–particle contact, we still want to highlight that all particles within a cluster have strong electrical coupling with negligible resistance compared to the resistance between adjacent clusters. The number of particles in a cluster of the few-layer films ranges from 2 to 20 (Fig. 4d, S5d, S5f and S5h) but the overview images indicate that they may consist of tens of particles (Fig. 4b and S5b).

The existence of strongly connected clusters is consistent with the formation process of the hybrid particle films. The original dispersion contains hybrid nanoparticles at a low concentration, where most of the particles are well dispersed.[21] When this dispersion is drop-cast and allowed to dry on the substrate, water evaporates and the particle concentration increases. Particles may accumulate at the gas–liquid or solid–liquid interfaces. Here, we assume adsorption of the particles at the solid interface as we observed a golden haze at the interface under the cast drop. If the interaction between the particles is dominated by the polymer shell and not the metal cores (shell-dominated[33]), the local concentration increase will lead to agglomeration once the solubility of the polymer in water is reached. Additional attractive contributions from the gold cores (that have large Hamaker constants) only accelerate this agglomeration process. The resulting agglomerates are still solvated. The polymer chains remain mobile and adjacent particles have the mobility and time to restructure such that the dense polymer and particle packings minimize their free energy. When almost all water has evaporated, strong capillary forces compress the agglomerates into a solidifying layer. Agglomerates are converted into the 2D clusters with strong electrical coupling that we observe. During this rapid transition, the mobility of the clusters is insufficient to arrange, also because they are larger and complex in shape. Only a few local contacts form between different clusters. As a result, the electrical resistance inside clusters is smaller than between clusters.

Some particles, which can be identified in the topography map of Fig. 4c, do not show any current signal in the corresponding current map in Fig. 4d, and they seem to be electrically disconnected from the conductive network. Additional imaging showed that sometimes clusters of many particles are similarly disconnected (Fig. S5 in the SI). Please note that the shape of each particle can be recognized in the current map in Fig. 4d, and that there is a spot of zero current in the center of each particle. The lack of current in the particles' center is an imaging artifact, which is a collective result of deposition of insulating materials on the tip apex and abrasion of the metal coating from the conductive tip apex. Degradation of the

metallic coating of conducting AFM tips and transfer of the polymeric material are two challenges in performing cAFM measurements.[34–36] The gradual decay of current at the center of individual nanoparticles in the course of repeated scanning in contact mode is shown in Fig. S6 in the SI along with the transmission electron microscopy (TEM) image of a used tip.

Nevertheless, the constant current level within each cluster of particles and across the circumference of each particle indicates that the tip–sample resistance is small compared to the contact resistance linking the group of particles to the overall network, except for the blocked spot in the center of each particle. It was previously observed that even one-dimensional chains of Au nanoparticles with conductive polymer shells show a similar constant current in cAFM images.[18]

Resistance maps corresponding to the current maps in Fig. 4d are presented in Fig. 4e and f with two different color scales to highlight different resistance regimes. For this few-layer film, there is no underlying network of particles and we can interpret the difference in path resistance between clusters of particles as the contact resistance of the electrical link between these clusters. This difference in resistance is typically as large as several tens of GΩ. Even the apparently low-resistance pathway from top to bottom in Fig. 4e (dark color) is found to have an electrically weak link of 10 GΩ resistance when using different color scales in Fig. 4f.

One may suspect that the high resistance of the links between clusters of particles is caused by layers of electrically insulating PVA, the material that was added to enhance the mechanical properties of the films. We have prepared few-layer films from low-concentration inks without PVA and found that the large resistance between clusters with equal current signals is not specific to PVA but occurs similarly in films without added PVA (see Fig. S7 in the SI). The resistance thus originates at the contact of unknown geometry between the shells of conducting polymers. This finding agrees with the macroscopic characterization results for the same bulk films, which showed that small amounts of PVA not only increase the mechanical stability of the films, but also increase conductivity. This increase in conductivity is probably a result of phase separation into a network of connected PEDOT-covered Au particles and a PSS-PVA matrix, which was revealed by small-angle X-ray scattering.[22]

Current maps as shown in Fig. 3 and 4 are stable and reproducible under repeated scanning with the tip. Furthermore, the bulk films and few-layer films exhibit the characteristic current maps with distinct islands of constant current magnitude after one year of storage. The configuration of particles or clusters which leads to a local variation of resistance to each measured point is thus as stable as the related inter-particle or inter-cluster resistances.

Conclusions

Topography and local electrical conductivity were measured simultaneously with single-nanoparticle resolution on an inkjet-printed film, produced from a conductive ink of Au nanoparticles with a PEDOT:PSS shell for stabilization and electric conduction and with PVA as an additive for mechanical stabilization. Despite the well-known instabilities and material transfers occurring during contact-mode AFM of polymeric materials, reproducible current maps were obtained. Imaging local variations in the resistance of the particle network was possible as the tip–sample resistance was smaller than the characteristic resistances within the network. The results confirm that conductive AFM is a viable method to study printed electronics in their technologically relevant form.

Our experiments revealed the existence of clusters that are electrically well connected with negligible inter-particle resistance. These clusters are connected to neighboring clusters by electrical links of higher contact resistance. We quantified local variations in the resistance and found that the contact resistance between topographically adjacent particles can take any value between a few hundreds of Ω and GΩ. Comparison with films produced without the PVA additive showed that the clustering of resistances and the higher contact resistances between clusters of particles are not induced by the non-conductive PVA but are consequences of the respective geometric configuration of particles and the structure of the conductive polymer shell.

The three-dimensional inkjet-printed films have an electrically well-connected network of particles, and only single particles or small groups of particles at the surface exhibit a contact resistance between a few hundreds of Ω to MΩ with respect to the conductive network. For comparison, we also studied very thin films of single- or few-layer particle thickness. The current maps of these two-dimensional films revealed a clustering of particles, which led to distinct clusters of electrically well-connected particles, but higher resistance up to GΩ between clusters and thus an overall low conduction of the network.

The results indicate that it might be difficult to obtain good conduction in two-dimensional few-layer films of hybrid particles, where clustering can weaken the electric connection between the local current networks and hamper the percolation of current pathways. We suggest that not only thicker films allow for better percolation along the additional geometric dimension, but also the denser local configuration of particles in a three-dimensional film may enhance the conductive coupling between the PEDOT:PSS shells, for example, by the alignment of π-stacked polymer chains.

Author contributions

S. D.: conceptualization, investigation, formal analysis, visualization, and writing – original draft. M. K.: resources and writing – review & editing. T. K.: conceptualization and writing – review & editing. R. B.: conceptualization, formal analysis, supervision, and writing – review & editing.

Conflicts of interest

There are no conflicts to declare.

Data availability

Data for this article, namely raw AFM data files, are available at Zenodo: https://doi.org/10.5281/zenodo.17350453.

Supplementary information (SI) is available. See DOI: https://doi.org/10.1039/d5nr04335b.

References

1 J. Kwak, W. K. Bae, M. Zorn, H. Woo, H. Yoon, J. Lim, S. W. Kang, S. Weber, H.-J. Butt, R. Zentel, S. Lee, K. Char and C. Lee, Characterization of Quantum Dot/Conducting Polymer Hybrid Films and Their Application to Light-Emitting Diodes, *Adv. Mater.*, 2009, **21**, 5022–5026.

2 N. Hirata, M. Sato, E. Tsunemi, Y. Watanabe, H. Tsunoyama, M. Nakaya, T. Eguchi, Y. Negishi and A. Nakajima, Fabrication and Characterization of Floating Memory Devices Based on Thiolate-Protected Gold Nanoclusters, *J. Phys. Chem. C*, 2017, **121**, 10638–10644.

3 F. Mathias, A. Fokina, K. Landfester, W. Tremel, F. Schmid, K. Char and R. Zentel, Morphology Control in Biphasic Hybrid Systems of Semiconducting Materials, *Macromol. Rapid Commun.*, 2015, **36**, 959–983.

4 C. Rossner, T. A. F. König and A. Fery, Hairy Plasmonic Nanoparticles, in *Hairy Nanoparticles*, 2023, pp. 351–374.

5 Y. Brasse, C. Ng, M. Magnozzi, H. Zhang, P. Mulvaney, A. Fery and D. E. Gómez, A Tunable Polymer–Metal Based Anti-Reflective Metasurface, *Macromol. Rapid Commun.*, 2020, **41**, 1900415.

6 J. H. M. Maurer, L. González-García, I. K. Backes, B. Reiser, S. M. Schlossberg and T. Kraus, Direct Nanoimprinting of a Colloidal Self-Organizing Nanowire Ink for Flexible, Transparent Electrodes, *Adv. Mater. Technol.*, 2017, **2**, 1700034.

7 H. W. Tan, J. An, C. K. Chua and T. Tran, Metallic Nanoparticle Inks for 3D Printing of Electronics, *Adv. Electron. Mater.*, 2019, **5**, 1800831.

8 A. Kamyshny, M. Ben-Moshe, S. Aviezer and S. Magdassi, Ink-Jet Printing of Metallic Nanoparticles and Microemulsions, *Macromol. Rapid Commun.*, 2005, **26**, 281–288.

9 I. Kanelidis and T. Kraus, The role of ligands in coinage-metal nanoparticles for electronics, *Beilstein J. Nanotechnol.*, 2017, **8**, 2625–2639.

10 J. Chung, S. Ko, N. R. Bieri, C. P. Grigoropoulos and D. Poulikakos, Conductor microstructures by laser curing of printed gold nanoparticle ink, *Appl. Phys. Lett.*, 2004, **84**, 801–803.

11 J. Perelaer, B.-J. de Gans and U.S. Schubert, Ink-jet Printing and Microwave Sintering of Conductive Silver Tracks, *Adv. Mater.*, 2006, **18**, 2101–2104.

12 M. Zorn, W. K. Bae, J. Kwak, H. Lee, C. Lee, R. Zentel and K. Char, Quantum Dot–Block Copolymer Hybrids with Improved Properties and Their Application to Quantum Dot Light-Emitting Devices, *ACS Nano*, 2009, **3**, 1063–1068.

13 M. Núñez-Martínez, E. Quiñoá and F. Freire, Stereocomplex Nanocomposite Switch Based on Dynamic Helical Polymer-Gold and Silver Nanoparticle Hybrid Materials, *Chem. Mater.*, 2023, **35**, 4865–4872.

14 Á.I López-Lorente, M. L. Soriano and M. Valcárcel, Analysis of citrate-capped gold and silver nanoparticles by thiol ligand exchange capillary electrophoresis, *Microchim. Acta*, 2014, **181**, 1789–1796.

15 A. Escudero, L. González-García, R. Strahl, D. J. Kang, J. Drzic and T. Kraus, Large-Scale Synthesis of Hybrid Conductive Polymer–Gold Nanoparticles Using "Sacrificial" Weakly Binding Ligands for Printing Electronics, *Inorg. Chem.*, 2021, **60**, 17103–17113.

16 J. Drzic, A. Escudero, L. González-García and T. Kraus, Sacrificial ligand route to hybrid polythiophene–silver nanoparticles for sinter-free conductive inks, *Inorg. Chem. Front.*, 2023, **10**, 1552–1560.

17 T. Minari, Y. Kanehara, C. Liu, K. Sakamoto, T. Yasuda, A. Yaguchi, S. Tsukada, K. Kashizaki and M. Kanehara, Room–Temperature Printing of Organic Thin–Film Transistors with π–Junction Gold Nanoparticles, *Adv. Funct. Mater.*, 2014, **24**, 4886–4892.

18 G. Yi, M. Hoffmann, S. Seçkin, T. A. F. König, I. Hermes, C. Rossner and A. Fery, Toward coupling across inorganic/organic hybrid interfaces: polyaniline-coated gold nanoparticles with 4-aminothiophenol as gold-anchoring moieties, *Colloid Polym. Sci.*, 2025, **303**, 1743–1751.

19 J. Delabie, J. De Winter, O. Deschaume, C. Bartic, P. Gerbaux, T. Verbiest and G. Koeckelberghs, Development of a Layered Hybrid Nanocomposite Material Using α,ω-Bifunctionalized Polythiophenes, *Macromolecules*, 2020, **53**, 11098–11105.

20 D. Tanaka, Y. Inuta, M. Sakamoto, A. Furube, M. Haruta, Y.-G. So, K. Kimoto, I. Hamada and T. Teranishi, Strongest π–metal orbital coupling in a porphyrin/gold cluster system, *Chem. Sci.*, 2014, **5**, 2007–2010.

21 B. Reiser, L. González-García, I. Kanelidis, J. H. M. Maurer and T. Kraus, Gold nanorods with conjugated polymer ligands: sintering-free conductive inks for printed electronics, *Chem. Sci.*, 2016, **7**, 4190–4196.

22 M. A. H. Klos, L. González-García and T. Kraus, Mechanically Robust, Inkjet-Printable Polymer Nanocomposites with Hybrid Gold Nanoparticles and Metal-like Conductivity, *ACS Appl. Mater. Interfaces*, 2024, **16**, 31576–31585.

23 D. Lanigan and E. Thimsen, Contact Radius and the Insulator–Metal Transition in Films Comprised of Touching Semiconductor Nanocrystals, *ACS Nano*, 2016, **10**, 6744–6752.

24 B. L. Greenberg, Z. L. Robinson, Y. Ayino, J. T. Held, T. A. Peterson, K. A. Mkhoyan, V. S. Pribiag, E. S. Aydil and U. R. Kortshagen, Metal-insulator transition in a semiconductor nanocrystal network, *Sci. Adv.*, 2019, **5**, eaaw1462.

25 Q. Chen, J. R. Guest and E. Thimsen, Visualizing Current Flow at the Mesoscale in Disordered Assemblies of Touching Semiconductor Nanocrystals, *J. Phys. Chem. C*, 2017, **121**, 15619–15629.

26 I. J. Fernandes, A. F. Aroche, A. Schuck, P. Lamberty, C. R. Peter, W. Hasenkamp and T. L. A. C. Rocha, Silver nanoparticle conductive inks: synthesis, characterization, and fabrication of inkjet-printed flexible electrodes, *Sci. Rep.*, 2020, **10**, 8878.
27 L. Sun, J. Wang and E. Bonaccurso, Conductivity of individual particles measured by a microscopic four-point-probe method, *Sci. Rep.*, 2013, **3**, 1991.
28 Z.-F. Cai, T. Chen and D. Wang, Insights into the Polymerization Reactions on Solid Surfaces Provided by Scanning Tunneling Microscopy, *J. Phys. Chem. Lett.*, 2023, **14**, 2463–2472.
29 Q. K. Ong, J. Reguera, P. J. Silva, M. Moglianetti, K. Harkness, M. Longobardi, K. S. Mali, C. Renner, S. D. Feyter and F. Stellacci, High-Resolution Scanning Tunneling Microscopy Characterization of Mixed Monolayer Protected Gold Nanoparticles, *ACS Nano*, 2013, **7**, 8529–8539.
30 M. Chaudhary, S. Dey, K. Date, S. B. Iyyer and C. V. Dharmadhikari, Electron Transport in Dodecylamine Capped Gold Nanocluster Films Using Current Sensing Atomic Force Microscope (C-AFM), *J. Nanosci. Nanotechnol.*, 2009, **9**, 5467–5470.
31 T. Hassenkam, K. Moth-Poulsen, N. Stuhr-Hansen, K. Norgaard, M. S. Kabir and T. Bjornholm, Self-assembly and conductive properties of molecularly linked gold nanowires, *Nano Lett.*, 2004, **4**, 19–22.
32 S. Magdassi, M. Grouchko, D. Toker, A. Kamyshny, I. Balberg and O. Millo, Ring stain effect at room temperature in silver nanoparticles yields high electrical conductivity, *Langmuir*, 2005, **21**, 10264–10267.
33 T. Kister, D. Monego, P. Mulvaney, A. Widmer-Cooper and T. Kraus, Colloidal Stability of Apolar Nanoparticles: The Role of Particle Size and Ligand Shell Structure, *ACS Nano*, 2018, **12**, 5969–5977.
34 Y. Yuan and M. Lanza, The Effect of Relative Humidity in Conductive Atomic Force Microscopy, *Adv. Mater.*, 2024, **36**, 2405932.
35 N. L. Tolman, R. Bai and H. Liu, Hydrocarbons in the Meniscus: Effects on Conductive Atomic Force Microscopy, *Langmuir*, 2023, **39**, 4274–4281.
36 L. Jiang, J. Weber, F. M. Puglisi, P. Pavan, L. Larcher, W. Frammelsberger, G. Benstetter and M. Lanza, Understanding Current Instabilities in Conductive Atomic Force Microscopy, *Materials*, 2019, **12**, 459.